Digital soil mapping based site-specific nutrient management in a sugarcane field in Burdekin

Author:
Li, N; Zhao, X; Wang, J; Sefton, M; Triantafilis, J

Publication details:
Geoderma
v. 340
pp. 38 - 48
0016-7061 (ISSN); 1872-6259 (ISSN)

Publication Date:
2019-04-15

Publisher DOI:
https://doi.org/10.1016/j.geoderma.2018.12.033

Geoderma 340 (2019) 38–48

Contents lists available at ScienceDirect

Geoderma

journal homepage: www.elsevier.com/locate/geoderma

Digital soil mapping based site-specific nutrient management in a sugarcane field in Burdekin

Nan Li[a], Xueyu Zhao[a], Jie Wang[a], Michael Sefton[b], John Triantafilis[a,*]

[a] School of Biological, Earth and Environmental Sciences, Faculty of Science, UNSW Sydney, Kensington, NSW 2052, Australia
[b] Herbert Cane Productivity Services Pty Ltd., Ingham, Qld 4850, Australia

ARTICLE INFO

Handling editor: Alex McBratney

Keywords:
Calcium
Magnesium
γ-Ray spectrometer
Electromagnetic induction
Regression kriging
Linear mixed model
Digital soil map
Nutrient management

ABSTRACT

In the highly productive Burdekin valley, the soil is heterogeneous. To optimise productivity, for irrigated crops such as sugarcane, essential nutrients such as calcium (Ca) and magnesium (Mg) need to be applied. To assist sugarcane farmers, nutrient management guidelines for these mineral elements have been recommended (i.e. Six-Easy-Steps) based on the exchangeable (Exch.) Ca and Mg. However, these are applied using 'one size fits all' approach, which lead to fertiliser use inefficiencies, given the alluvial nature of the landscape; where sandy soil characterises the ephemeral creeks (Chromosols) and clay soil types (Sodosols and Vertosols) of the plains. Herein we used and compared regression kriging (RK) and linear mixed models (LMM) to create digital soil maps (DSM). We also compared the efficacy of various proximal sensed γ-ray spectrometry and EM data. Using measures of bias (mean error - ME) and precision (root mean squared error - RMSE) of predictions, as well as the Lin's concordance, we determine which model and data was most useful using a leave-one-out cross-validation. The results for Exch. Ca showed that while RK approach had a strong concordance (0.81), unbiased (0.01) and precise (0.06), the LMM outperformed RK, given the better concordance (0.87) and bias (0.00). The MSPE of the final LMM DSM (0.01) was also smaller compared to the RK DSM (0.0123). Moreover, both DSM was superior to the traditional Soil Order map (0.0171). The results for Exch. Mg were equivalent. We also conclude, that while good concordance was achieved using either γ-ray (Lin's = 0.79) or EM (0.83) for Exch. Ca, using both proximal sensors was optimal. The results showed that pedometric approach can be used to generate a DSM of Exch. Ca and Mg in a sugarcane field. In terms of soil use and management, the infertile sandy textured soil associated with the prior stream channels and characterised by small Exch. Ca (< 0.2 cmol(+)/kg) and Mg (< 0.5 cmol (+)/kg), require large fertiliser rates of lime (3 t/ha) and magnesium sulphate (150 kg/ha), respectively. Conversely, variable amounts of fertiliser rates of lime (2.5 and 2 t/ha) and magnesium sulphate (125, 100 and 75 kg/ha), were required for the clayier soil types associated with the Sodosols (2Dyb) and Vertosols (2Uge).

1. Introduction

In the highly productive Burdekin valley, soil is heterogeneous (Prosser et al., 2002); owing to the alluvial nature of the landscape, where sandy textures characterise ephemeral water-courses and fine-textured clays define flood plain. To optimise productivity, essential nutrients such as calcium (Ca) and magnesium (Mg) need to be applied differentially in these areas. This is specifically the case for sugarcane production, whereby Ca is important for sugarcane growth and development (Hepler, 2005), given it is required for structural in the cell and wall. It also can neutralize excess acid or alkaline soil, which is key to proper sugarcane root growth (White and Broadley, 2003). Without this sugarcane is susceptible to drought and improper mineral nutrition (Bakker, 2012). In terms of magnesium (Mg), it is essential for sugarcane to harvest solar energy and drive photochemistry (Beale, 1999; Solymosi and Schoefs, 2008) because it is the central component of the chlorophyll molecule. In this way, Mg is considered a major player in N uptake and utilisation (Gastal and Lemaire, 2002; Grzebisz, 2013).

Given the importance of Ca and Mg in the soil, the industry developed nutrient management guidelines for these mineral elements as part of the Six-Easy-Steps for nutrient management (Schroeder et al., 2009), in the Burdekin; a joint initiative of the Queensland Department of Environment and Resource Management (DERM) and Sugar Research Australia. For example, to ensure the adequate supply of Ca to the soil, application rates of lime were recommended based on soil exchangeable (Exch.) Ca. For example, when Exch. Ca is small (< 0.2 cmol(+)/kg), the lime application rate should be 3 t/ha

* Corresponding author.
E-mail address: j.triantafilis@unsw.edu.au (J. Triantafilis).

https://doi.org/10.1016/j.geoderma.2018.12.033
Received 8 August 2018; Received in revised form 26 November 2018; Accepted 17 December 2018
0016-7061/

Table 1
Six-Easy-Steps Nutrient management guidelines for sugarcane in the Burdekin district.

Range	Exch. Ca (cmol(+)/kg)	Lime (tonnes/ha)	Exch. Mg (cmol(+)/kg)	Magnesium (kg/ha)
Small	< 0.2	3	< 0.05	150
Intermediate-small	0.2–0.4	2.5	0.05–0.1	125
Intermediate	0.4–0.6	2	0.1–0.15	100
Intermediate-large	0.6–0.8	1.5	0.15–0.2	75
Large	> 0.8	1	> 0.2	50

(Table 1). Conversely, when the Exch. Ca is considered large (> 0.8 cmol(+)/kg) the rate of application would be 1 t/ha. Similarly, and for Mg, the guidelines suggest for small (< 0.05 cmol(+)/kg) and large (> 0.2 cmol(+)/kg) Exch. Mg, rates of application should be 150 and 50 kg/ha, respectively. However, accounting for the spatial variation of Exch. Ca and Mg requirements across a given field is problematic owing to time consuming, labour intensive and prohibitive cost of soil sampling and laboratory analysis.

A pedometric approach, such as creating a digital soil map (DSM), can potentially be applied (McBratney et al., 2003; Huang et al., 2014). That is, we can collect several soil samples for laboratory analysis (i.e. Exch. Ca and Mg) and relate these to easier to acquire proximal sensed data that reveal a close relationship, using statistical models (Rossel et al., 2006; Minasny and Hartemink, 2011). In terms of proximal sensed data, gamma-ray (γ-ray) spectrometer and electromagnetic (EM) induction data may be useful. This is because many authors have found that these data could be used to establish a direct relationship with soil properties related to Exch. Ca and Mg, such as clay and cation exchange capacity (CEC). For example, Bishop and McBratney (2001) exploited the correlation between topsoil (0–0.15 m) CEC and EM at the field scale to develop a map using regression kriging (RK). Triantafilis et al. (2009) used a similar approach to relate EM data to average profile (0–2 m) CEC. More recently, Nelson et al. (2011) used a Linear Mixed Model (LMM) to combine γ-ray and EM data collected across a large area to map clay, whereas Li et al. (2018) combined γ-ray and EM data in a field to model deterministic trend in the variation of topsoil (0–0.30 m) and subsoil (0.6–0.9 m) CEC using a Bayesian approach.

Given the often-strong relationship between γ-ray and EM data with clay and CEC, a major objective of this paper was to determine if an equivalent relationship existed between proximal sensed data and Exch. Ca and Mg. We then aim to compare various mathematical modelling approaches (RK and LMM) and test the usefulness of any such relationships to make DSM; using measures such as precision (root mean square error - RMSE), bias (mean error - ME) and concordance (Lin's). We also calculate the means square prediction error (MSPE) of the final DSM and compare these to a traditionally generated soil map of Soil Orders (Donnollan et al., 1990). We also compare the two proximal sensed data sets to determine which is superior in terms of these measures of prediction if used alone to develop a DSM. To provide a practical demonstration of the soil use and management implications, we also determined the fertilisers requirement for Exch. Ca (i.e. lime) and Exch. Mg and in accord with respect to the Six-Easy-Steps for Burdekin nutrient management (Schroeder et al., 2009).

2. Materials and methods

2.1. Study field

The study field was located 24 km to the west of Ayr, in the Burdekin River Irrigation Area (BRIA), North Queensland (Fig. 1a). The environmental and climatic conditions of BRIA are ideal for sugarcane (*Saccharum officinarum*) growing and the region has a reputation of being one of the highest yielding sugarcane areas in Australia (Bristow et al., 2000). The study field was 900 m long and 400 m wide (Fig. 1b), with an approximate area of 32 ha. The sugarcane is grown in north-south aligned beds. The climate is warm and sub-humid, with well-defined wet and dry seasons (Stokes et al., 2006). The annual rainfall is 1032 mm, with over 50% of the total falling between December and March wet season. The summer temperature is high with maximums of 32.1 °C (December) and minimums of 11.8 °C (July).

The study field is characterised by Quaternary flood plain alluvium (Qa), predominantly fine-textured (clays) Burdekin River floodplains with littoral deposits near old streamlines (Christian et al., 1953). According to the soil survey report of Burdekin (Donnollan et al., 1990), at the northern end of study field, as shown in Fig. 1b, the soil is primarily a relict levee (6Dya) defined by sand or loam over friable or earthy clay and the soil types were a Chromosols according to Australian Soil Classification (Isbell, 2016). Immediately to the south, the soil has previously been described as yellow-grey duplex soils (6Dye) with sand or loam over sodic clay (Sodosols) and a hard setting surface. Next to south is the soil of the Burdekin River alluvial plain characterised by Vertosols (2Uge), which have a light to light-medium clay surfaces. These exhibit self-mulching characteristics. At the southern end, the soil is identified as yellow and yellow-grey duplex soils (2Dyb) with sand or loam over sodic clay (Sodosols) and profile strongly alkaline by 0.3 m (Sodosols).

2.2. Proximal sensed data collection

Two types of proximal sensed data were collected. The γ-ray spectrometry provides a direct measurement of natural gamma radiation from the top 0–0.3 m of the soil (Bierwith, 1996). A Radiation Solutions RS-700 (Mississauga, Ontario, Canada) instrument was mounted on a bracket and on the front of a 4WD vehicle. It was designed to collect the natural radioactive emissions of γ-rays from the following windows and for radioelements of K (1.37–1.57 MeV), U (1.66–1.86 MeV), Th (2.41–2.81 MeV) and across the whole spectrum (0.41–2.81 MeV). Detection is achieved with a crystal pack (RSX-1) with measurements of K in percentage (%), U and Th (parts per million - ppm) and TC (counts per second - CPS).

The second set of proximally sensed data was apparent electrical conductivity (EC_a) collected using a DUALEM-421S instrument (Mississauga, Ontario, Canada) which was positioned 0.3 m above the ground and strapped onto a PVC sled located behind the 4WD. The DUALEM-421S operates at a low frequency (9 kHz), incorporating horizontal co-planar (HCP) and perpendicular (PRP) receiver arrays. The distance between the transmitter to the HCP receivers are 1, 2 and 4 m, giving theoretical EC_a depths of exploration (DOE) of 0–1.5 m (1mHcon), 0–3 m (2mHcon) and 0–6 m (4mHcon), respectively. The distances between the transmitter to the PRP receivers are 1.1, 2.1 and 4.1 m, which gives theoretical EC_a DOE of 0–0.5 m (1mPcon), 0–1 m (2mPcon) and 0–2 m (4mPcon), respectively.

Fig. 1c shows the data were acquired along 51 transects and with the instruments directly orientated over the beds. It should be noted that the first 6 transects, the DUALEM-421S data was collected without the use of a stabilising rope to keep the instrument positioned above the seed bed. The data were collected on August 17, 2017. In terms of raw data, 16,945 points were collected with the γ-ray spectrometer and 16,228 points were measured for EC_a. To co-locate the γ-ray and EC_a, we interpolated these data, using the VESPER (Minasny et al., 2005) package, onto a common 5 × 5 m grid by ordinary kriging (OK) using a neighbourhood of 20–30 points and a local variogram.

2.3. Soil sampling and laboratory analysis

Fig. 1d shows that a total 182 points were sampled. These points were located on 13 approximately equidistantly (30 m) transects selected from the 51 transects of proximally sensed data and on a proximately square grid with an interval of 35 m. At each points, soil samples were collected at a depth of 0–0.15 m. The samples were air-

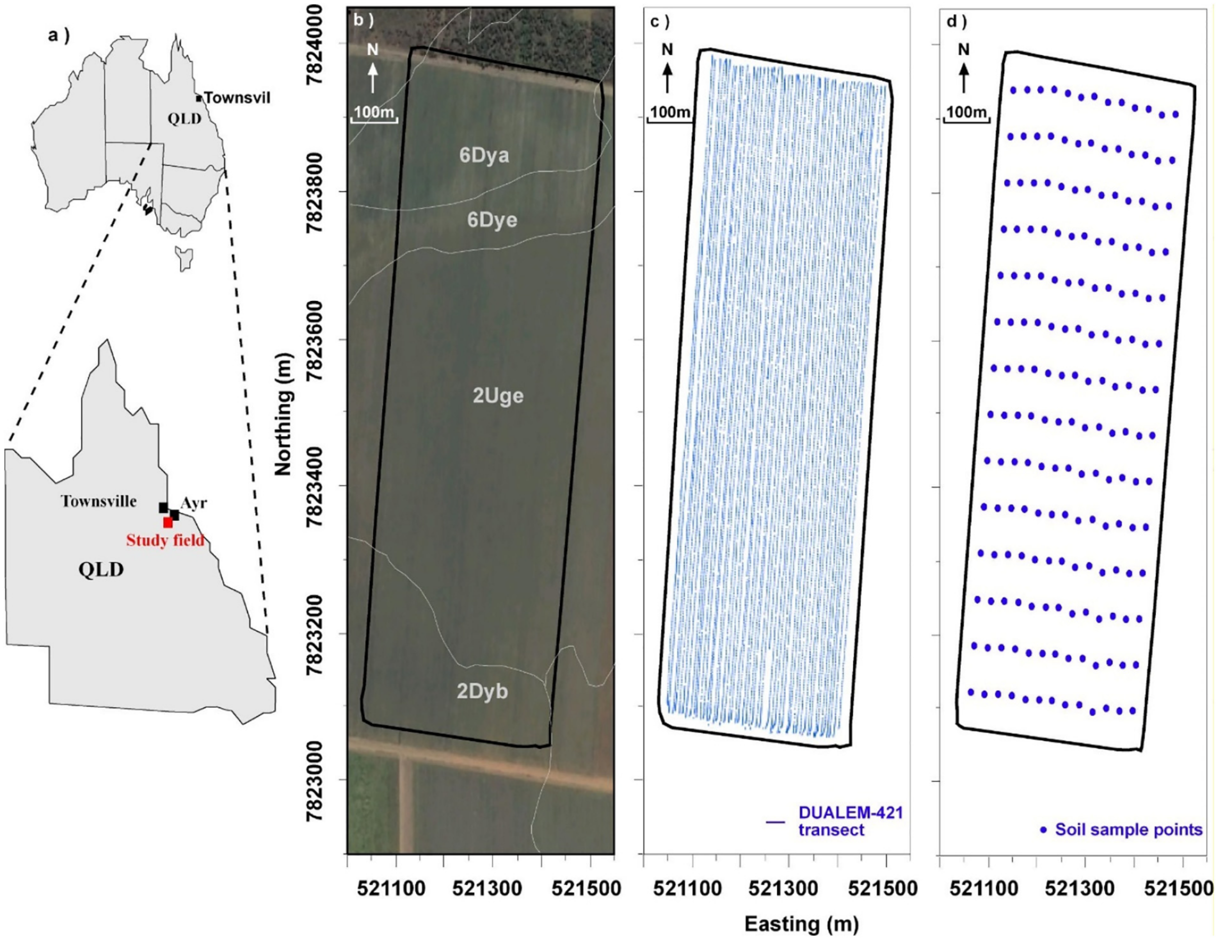

Fig. 1. (a) Location of the study field, (b) aerial photo of study field with Soil Order map (Donnollan et al., 1990), (c) spatial location of proximal sensed data survey transects, and (d) 182 soil sampling points.

Table 2
Summary statistics of measured soil exchangeable calcium (Exch. Ca - cmol(+)/kg), magnesium (Exch. Mg - cmol(+)/kg), proximal sensed gamma-ray (γ-ray) spectrometry and apparent electrical conductivity (EC_a) data at 182 sampling points and Pearson's correlation coefficient (r).

	Min	Mean	Median	Max	SD	Skewness	Kurtosis	CV (%)
Exch. Ca (cmol(+)/kg)	0.02	0.29	0.32	0.52	0.13	−0.58	−0.62	43.93
Exch. Mg (cmol(+)/kg)	0.00	0.09	0.10	0.21	0.05	−0.22	−0.59	50.42
K (%)	0.37	0.58	0.57	0.78	0.09	0.13	−0.34	15.70
U (ppm)	4.00	15.35	15.02	27.02	4.33	0.09	0.00	28.18
Th (ppm)	9.00	25.24	26.02	39.06	6.38	−0.15	−0.55	25.26
TC (cps)	478.34	601.48	614.75	696.91	50.20	−0.70	−0.31	8.346
1mPcon (mS/m)	3.5	26.30	29.85	45.4	11.32	−0.78	−0.56	43.05
1mHcon (mS/m)	8.2	63.87	70.4	112.8	27.56	−0.71	−0.59	43.14
2mPcon (mS/m)	6.6	57.26	64	100.4	25.03	−0.73	−0.59	43.73
2mHcon (mS/m)	18.2	95.94	105.05	170.4	39.11	−0.57	−0.67	40.77

Pearson's r	Exch. Ca	Exch. Mg	Clay	CEC
Exch. Ca	1			
Exch. Mg	0.92***	1		
Clay	0.77***	0.71***	1	
CEC	0.99***	0.96***	0.76***	1
K (%)	−0.46***	−0.41***	−0.50***	−0.45***
U (ppm)	0.49***	0.42***	0.41***	0.48***
Th (ppm)	0.41***	0.41***	0.51***	0.42***
TC (cps)	0.72***	0.64***	0.74***	0.71***
1mPcon (mS/m)	0.85***	0.81***	0.89***	0.85***
1mHcon (mS/m)	0.82***	0.77***	0.90***	0.82***
2mPcon (mS/m)	0.83***	0.79***	0.90***	0.83***
2mHcon (mS/m)	0.79***	0.74***	0.90***	0.79***

Note: **, < 0.01, ***, < 0.001.

Table 3
Summary statistics of kriged proximal sensed gamma-ray (γ-ray) spectrometry and apparent electrical conductivity (EC_a) data at 13690 grid points.

	Min	Mean	Medium	Max	SD	Skewness	Kurtosis	CV (%)
K (%)	0.42	0.57	0.55	0.79	0.05	1.01	0.41	9.43
U (ppm)	5.55	15.53	16.25	25.13	2.39	−0.83	0.12	15.40
Th (ppm)	10.73	24.97	26.54	40.05	4.218	−1.06	0.06	16.89
TC (cps)	459.33	602.34	616.36	694.48	43.29	−1.04	−0.12	7.186
1mPcon (mS/m)	2.4	26.81	30.26	51.72	11.65	−0.78	−0.61	43.29
1mHcon (mS/m)	6.16	64.58	72.87	115.2	27.965	−0.72	−0.65	43.30
2mPcon (mS/m)	4.67	58.01	65.48	105.17	25.39	−0.75	−0.63	43.77
2mHcon (mS/m)	15.65	96.68	107.36	174.45	39.33	−0.66	−0.71	40.68

Pearson's r	K	U	Th	TC	1mPcon	2mPcon	1mHcon	2mHcon
K (%)	1							
U (ppm)	−0.71***	1						
Th (ppm)	−0.77***	0.82***	1					
TC (cps)	−0.70***	0.87***	0.90***	1				
1mPcon (mS/m)	−0.74***	0.78***	0.84***	0.85***	1			
1mHcon (mS/m)	−0.73***	0.78***	0.84***	0.86***	0.99***	1		
2mPcon (mS/m)	−0.73***	0.78***	0.84***	0.86***	0.99***	0.99	1	
2mHcon (mS/m)	−0.71***	0.77***	0.83***	0.86***	0.97***	0.99	0.99	1

Note: **, < 0.01, ***, < 0.001.

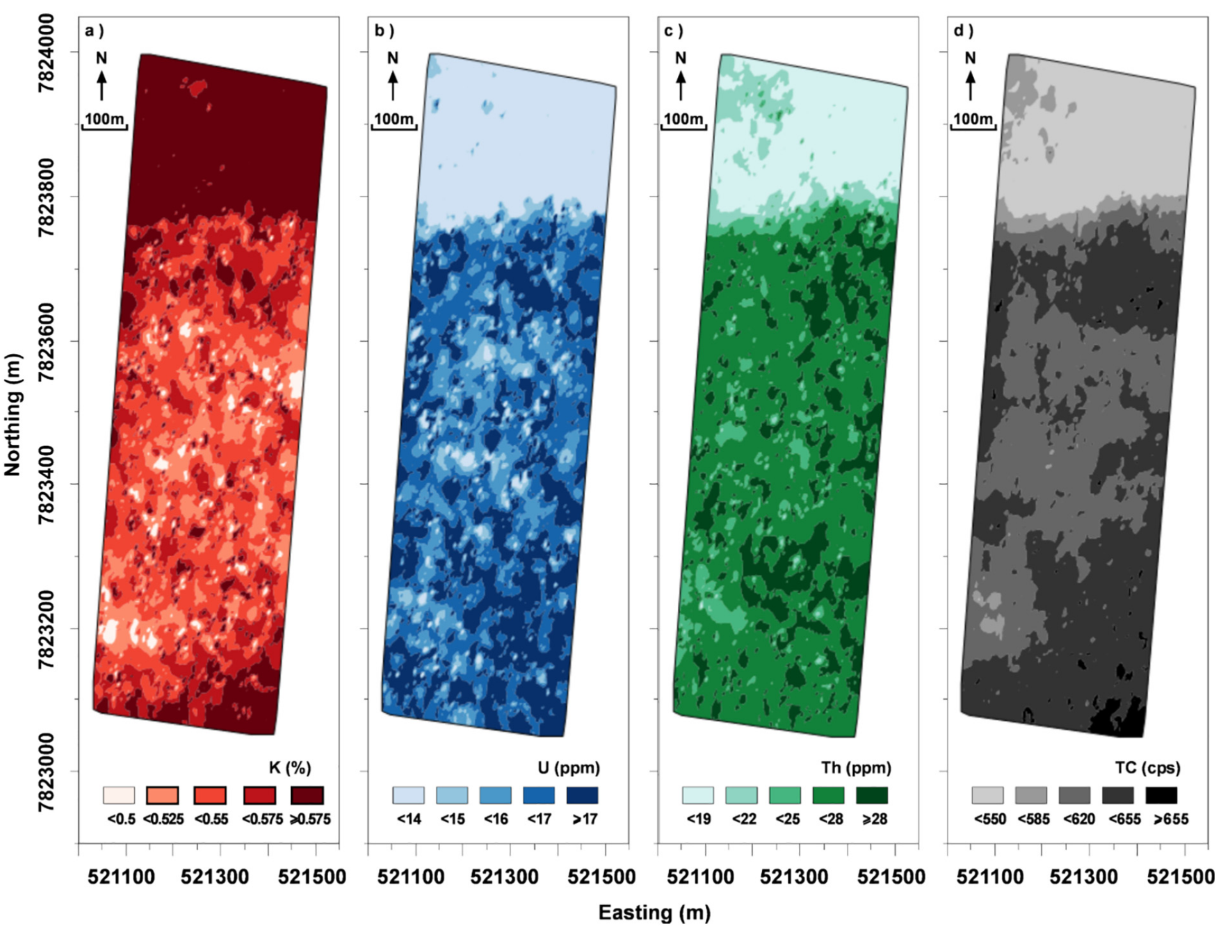

Fig. 2. Spatial distribution of kriged proximal sensed gamma-ray (γ-ray) spectrometry data including (a) potassium (K - %), (b) uranium (U - parts per million), (c) thorium (Th - parts per million) and (d) total count (TC - counts per second).

dried, crushed and passed through a 2-mm sieve before measurement. The extraction of Exch. Ca and Mg were followed Tucker's (1974) method by using a leaching device (Holmgren et al., 1977). Sample was washed with 60% ethanol to remove soluble salts, and the cations were displaced with 1 M NH_4Cl. The extracts were analysed using an inductively coupled plasma optical emission spectrometry (ICP-OES).

2.4. Modelling approaches

2.4.1. Regression kriging

Regression kriging (RK, Odeha et al., 1995) is a hybrid spatial modelling technique that combines two approaches: fit the explanatory variation using regression analysis and fit the residuals using ordinary

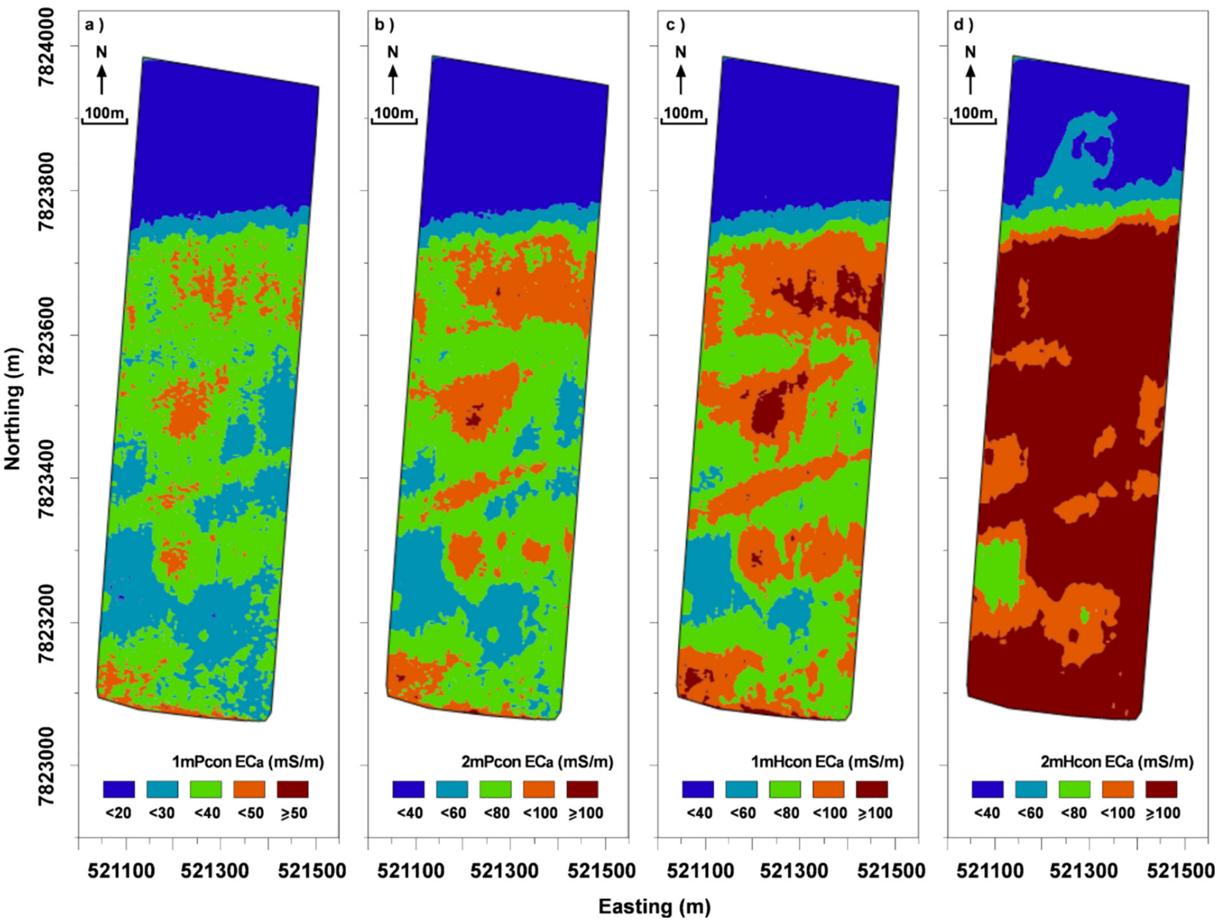

Fig. 3. Spatial distribution of kriged proximal sensed electrical conductivity (EC_a - m/Sm) data including (a) 1mPcon, (b) 2mPcon, (c) 1mHcon and (d) 2mHcon.

Table 4
Summary statistics of selected proximal sensed data, including gamma-ray (γ-ray) (e.g. Uranium-U [ppm] and Total Counts-TC [cps]) and apparent electrical conductivity (EC_a) (e.g. 1mPcon and 2mPcon) data used in a) regression kriging (RK) and b) linear mixed model (LMM) approach for predicting soil exchangeable calcium (Exch. Ca-cmol(+)/kg) and their probability values.

	Estimates	Standard error	t value	Prob > |t|
a) RK				
Intercept	−0.1878	0.0769	−2.443	0.02
U	0.0039	0.0012	3.195	0.00
TC	0.0004	0.0015	2.331	0.02
1mPcon	0.0158	0.0034	4.666	0.00
2mPcon	−0.0037	0.0015	−2.401	0.02
b) LMM				
Intercept	0.0241	0.0642	0.376	0.71
U	0.0041	0.0012	3.516	0.00
1mPcon	0.0077	0.0008	9.996	0.00

Table 5
Summary statistics of selected proximal sensed data, including gamma-ray (γ-ray) (e.g. Uranium-U [ppm] and Total Counts-TC [cps]) and apparent electrical conductivity (EC_a) (e.g. 1mPcon and 2mPcon) data used in a) regression kriging (RK) and b) linear mixed model (LMM) approach for predicting soil exchangeable magnesium (Exch. Mg-cmol(+)/kg) and their probability values.

	Estimates	Standard error	t value	Prob > |t|
a) RK				
Intercept	−0.0062	0.0080	−0.768	0.44
U	0.0011	0.0005	2.107	0.03
1mPcon	0.0062	0.0011	5.909	0.00
2mPcon	−0.0012	0.0004	−2.813	0.01
b) LMM				
Intercept	−0.0670	−0.0054	−1.248	0.21
TC	0.0001	0.0001	2.206	0.02
2mPcon	0.0001	0.0002	6.177	0.00

kriging (Hengl et al., 2004). Simply, a soil property of interest y at an unsampled points x_0 is predicted by summing the regressed values and kriged residuals (Odeha et al., 1994):

$$y(x_0) = f(x_0) + \varepsilon(x_0) \tag{1}$$

where $f(x_0)$ is the regressed value, and $\varepsilon(x_0)$ is the kriged residual that represent the uncertainty or errors which can calculated from the equation:

$$\varepsilon(x) = \sum_{i=1}^{n} w_i(x_0) \times \varepsilon(x_i) \tag{2}$$

where $w_i(x_0)$ are the kriging weights determined by the spatial dependence structure of the residual and $\varepsilon(x_i)$ is the regression residuals at points x_i.

Herein, we first established a relationship between the soil properties of interest (i.e. Exch. Ca and Mg) and the proximal sensed data (i.e., γ-ray and EM) at the sample points (182). This relationship was applied to the unvisited points (5 × 5 m grid) using the kriged value of the proximal sensed data at these points. In the second step, the residuals of the regression at the sample points were calculated. These residuals were kriging (ordinary) to the 5 × 5 m grid (Odeha et al., 1994). Both the regressed values and kriged residuals were then added together.

2.4.2. Linear mixed model

Linear mixed model (LMM) is an extension of a simple linear model,

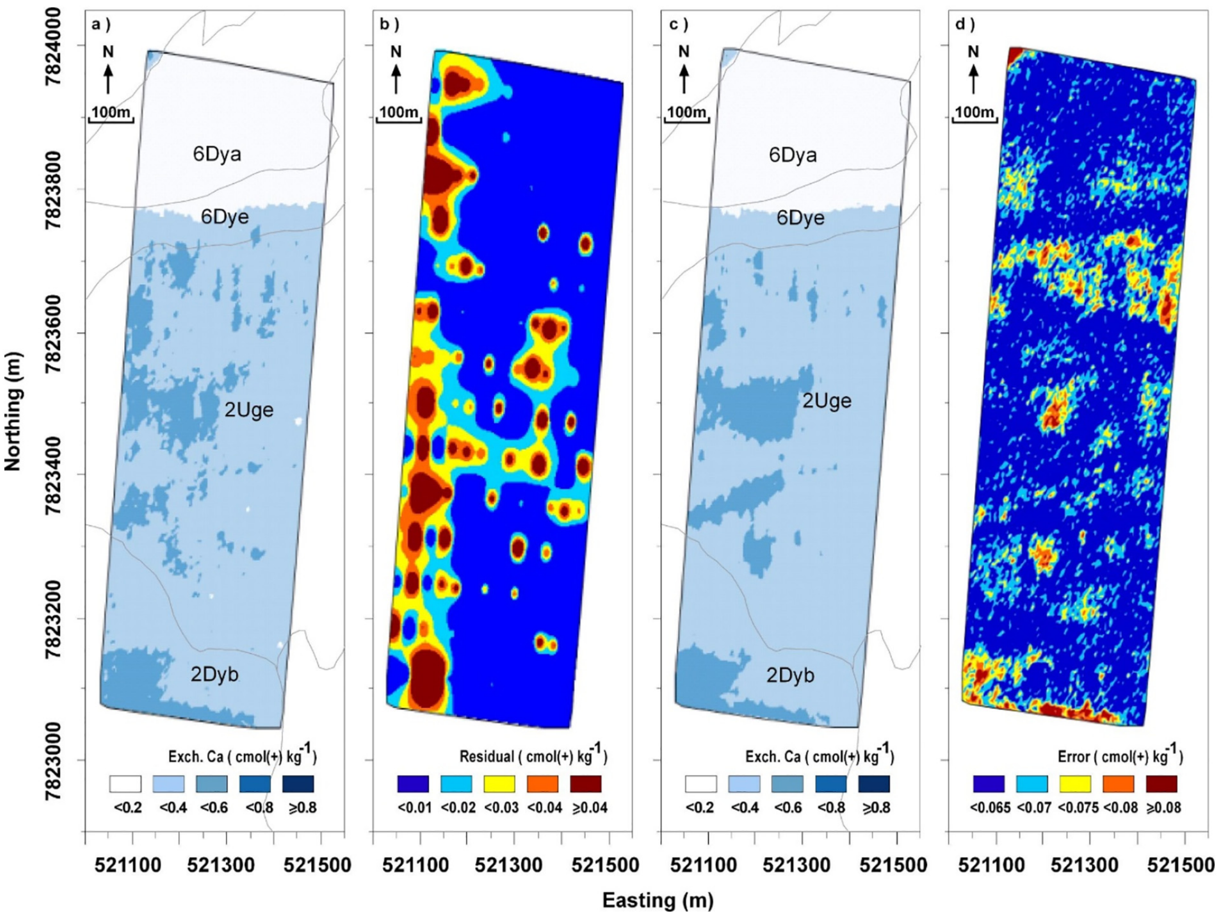

Fig. 4. Spatial distributions of predicted soil exchangeable calcium (Exch. Ca - cmol(+)/kg) using (a) regression kriging (RK) and (c) linear mixed model (LMM) and (b) spatial distributions of residuals of RK and (d) errors of LMM.

composed of a fixed effect component $X\tau$, which is the relationship between soil property (e.g. Exch. Ca and Mg) and the proximal sensed data (i.e., γ-ray and EM), a spatial correlation model (i.e. variogram), which was used to model the spatial dependence, the random effect (Zu), and an error component (ε). Generally, a LMM has the following form (Lark and Cullis, 2004):

$$y = X\tau + Zu + \varepsilon \tag{3}$$

where y is a vector of the observed response (i.e. Exch. Ca and Mg); X is a matrix of predictor variables (i.e., γ-ray and EM) at the observation points, whereby the vector τ contains the fixed-effects regression coefficients; Z is a design matrix for the random effects. The vectors u and ε contain random errors which are spatially correlated such that

$$\begin{bmatrix} u \\ \varepsilon \end{bmatrix} \sim \mathrm{N}\begin{pmatrix} \xi\sigma^2 G & 0 \\ 0 & \sigma^2 I \end{pmatrix} \tag{4}$$

where G is the correlation matrix where the correlation depends only on the relative point of the observations. I is the identity matrix and σ^2 is the variance of the independent error and ξ is the ratio of the variance of u to σ^2 (Lark et al., 2006).

2.4.3. Assessment of method performance

To compare the performance of modelling approach (i.e. RK and LMM) and proximal sensed data (i.e. γ-ray and EM), a leave-one-out cross-validation (Pebesma and Wesseling, 1998) was used. The principle of cross-validation is to leave out the measured value (i.e. Exch. Ca or Mg) at one point and then re-estimate it. Here, the performance of these approaches and proximal sensed data was assessed by identifying the Lin's concordance (Lawrence and Lin, 1989), mean error (ME) and the root mean squared error (RMSE) of prediction. The Lin's concordance coefficient can be calculated as:

$$\rho_c = \frac{2\rho\sigma_y\sigma_{\hat{y}}}{\sigma_y{}^2 + \sigma_{\hat{y}}{}^2 + (\mu_y - \mu_{\hat{y}})^2} \tag{5}$$

where y and $\hat{y}$ are the measured and predicted Exch. Ca or Mg; ρ is the correlation coefficient (Pearson's r) between measured and predicted data; σ_y and $\sigma_{\hat{y}}$ are the corresponding variances and μ_y and $\mu_{\hat{y}}$ are the means for the measured and predicted data. The ME is:

$$ME = \frac{1}{n}\sum_{t=1}^{n}(y_i - \hat{y}_i) \tag{6}$$

the RMSE is:

$$RMSE = \sqrt{\frac{1}{n}\sum_{t=1}^{n}(y_i - \hat{y}_i)^2} \tag{7}$$

If the model accurately describes the data, the Lin's concordance should be close to 1 for a good prediction and RMSE should be approximately equal to the standard deviation. For an unbiased prediction (centred on the true values) the ME should be near zero. All the calculation was conducted on the R platform.

We also calculated the mean squared prediction error (MSPE) of the DSM developed using RK and LMM and for both proximal sensed data as well as for the DSM developed using only the γ-ray or EM data as follows:

$$MSPE = \mathrm{E}[\{y_i - \hat{y}_i\}^2] \tag{8}$$

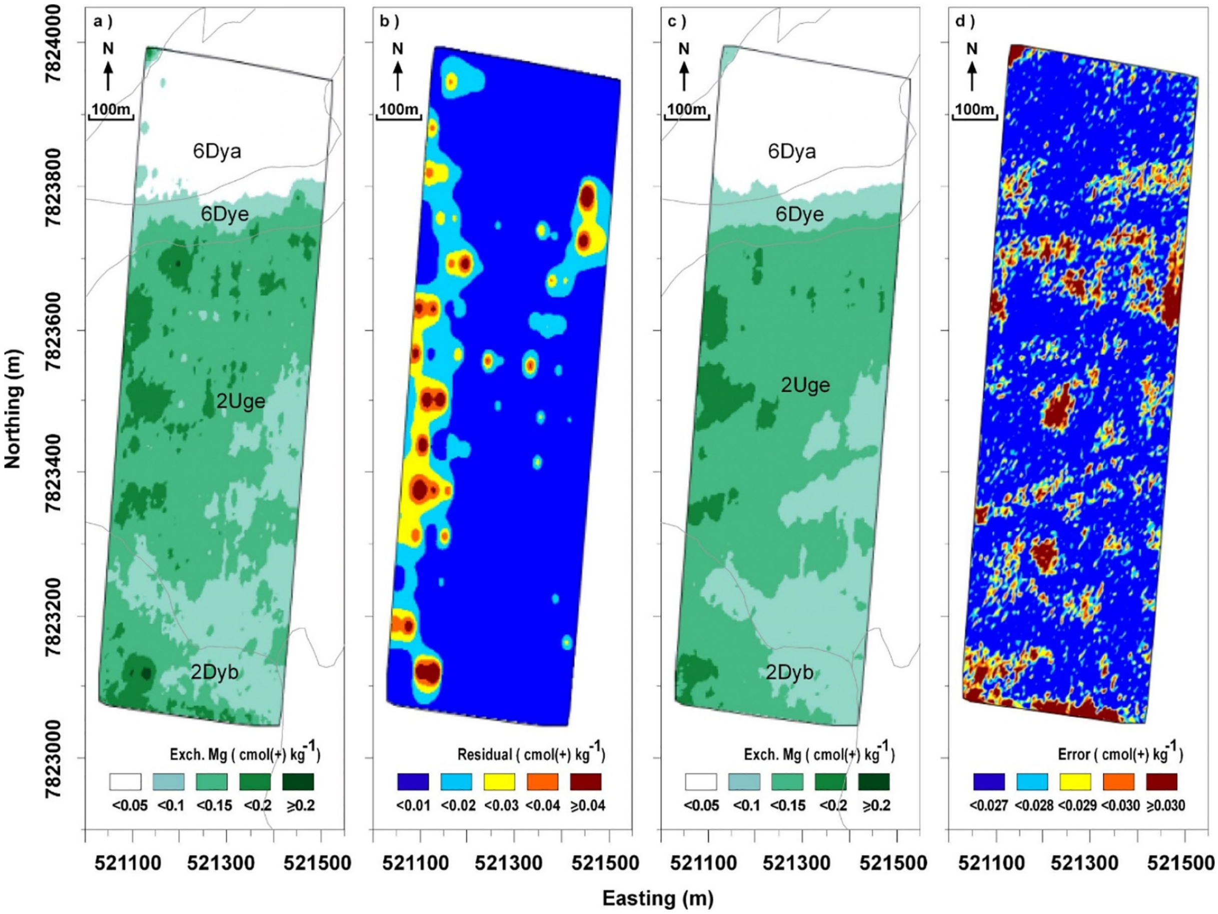

Fig. 5. Spatial distributions of predicted soil exchangeable magnesium (Exch. Mg - cmol(+)/kg) using (a) regression kriging (RK) and (c) linear mixed model (LMM) and (b) spatial distributions of residuals of RK and (d) errors of LMM.

To compare these maps with the map of the Soil Order map we calculated the MSPE of this map using:

$$MSPE = \sigma_i^2(1 + 1/n_i) \tag{9}$$

where $\sigma_i{}^2$ is the variance of the predicted Exch. Ca or Mg with soil order i and the mean of soil order i was estimated from n_i independently and randomly selected observations within the soil order (Brus and Lark, 2013).

3. Results and discussion

3.1. Exploratory data analysis

Table 2 shows the summary statistics of the measured Exch. Ca and Mg at 182 sampling points. The Exch. Ca varied from small (i.e. 0.02 cmol(+)/kg) to intermediate (i.e. 0.52 cmol(+)/kg) with the mean and median intermediate-small (i.e. 0.29 and 0.32 cmol(+)/kg, respectively). Given the skewness (−0.577) was < 1 (Oliver and Webster, 2014), the Exch. Ca was considered normally distributed. The coefficient of variation (CV) was large (43.93%), indicating the distribution of Exch. Ca has a high variation relative to the mean. In terms of Exch. Mg, it ranged from small (0.00 cmol(+)/kg) to large (0.21 cmol(+)/kg), with mean (0.09 com(+)/kg) and median (0.10 com(+)/kg) being about the same. The Exch. Mg was not skewed (−0.22) and had slightly higher variation (CV = 50.42%).

Table 2 also shows the Pearson's correlation coefficient (r) between soil properties and the proximal sensed data with Exch. Ca and Mg. Regarding the soil properties, the clay had a good correlation with Exch. Ca (0.77) and Mg (0.71), while larger coefficients can be found between CEC and both Exch. Ca (0.99) and Mg (0.96). With respect to the correlation coefficients between Exch. Ca and the γ-ray data, these were generally small, with the largest between TC (0.72), followed by U (0.49) with a negative correlation with K (−0.46). The correlations with Exch. Mg were similar, but slightly smaller. In all cases, the correlations were significant (***$P < 0.001$).

Table 3 shows the summary statistics of the kriged proximal sensed data. In general, the data statistics were consistent to the raw data (Table 2). The correlations between the EC_a data was much stronger with 1mPcon (0.99) and 2mPcon (0.97).

3.2. Spatial distribution of kriged proximal sensed data

Fig. 2 shows the spatial distribution of the kriged γ-ray data. In Fig. 2a, the large (≥0.575%) K predominantly characterises the northern and the south - east corner of the field. At the northern end of the field, the large K coincides with the topsoil sand or loam textured Chromosols. Conversely, the central and south were for the most part intermediate-small (< 0.525%) to intermediate-large (0.525–0.575%), which are related to the topsoil sand or loam over sodic clay (Sodosols) and the depressions characterised by Vertosols, which have a light to light-medium clay surfaces (A1), respectively. As shown in Fig. 2b, the opposite pattern was true for U (ppm); whereby the northern end had small values (< 14 ppm) while the intermediate-small (14–15 ppm) to large values (> 17 ppm) defined the centre and south. The distributions of Th (Fig. 2c) and TC (Fig. 2d) were similar to U.

Fig. 3 shows the spatial distribution of the kriged EC_a measured by different DUALEM-421S coil arrays. In Fig. 3a, the small 1mPcon values (< 20 mS/m) was mainly distributed in the north, while to the south

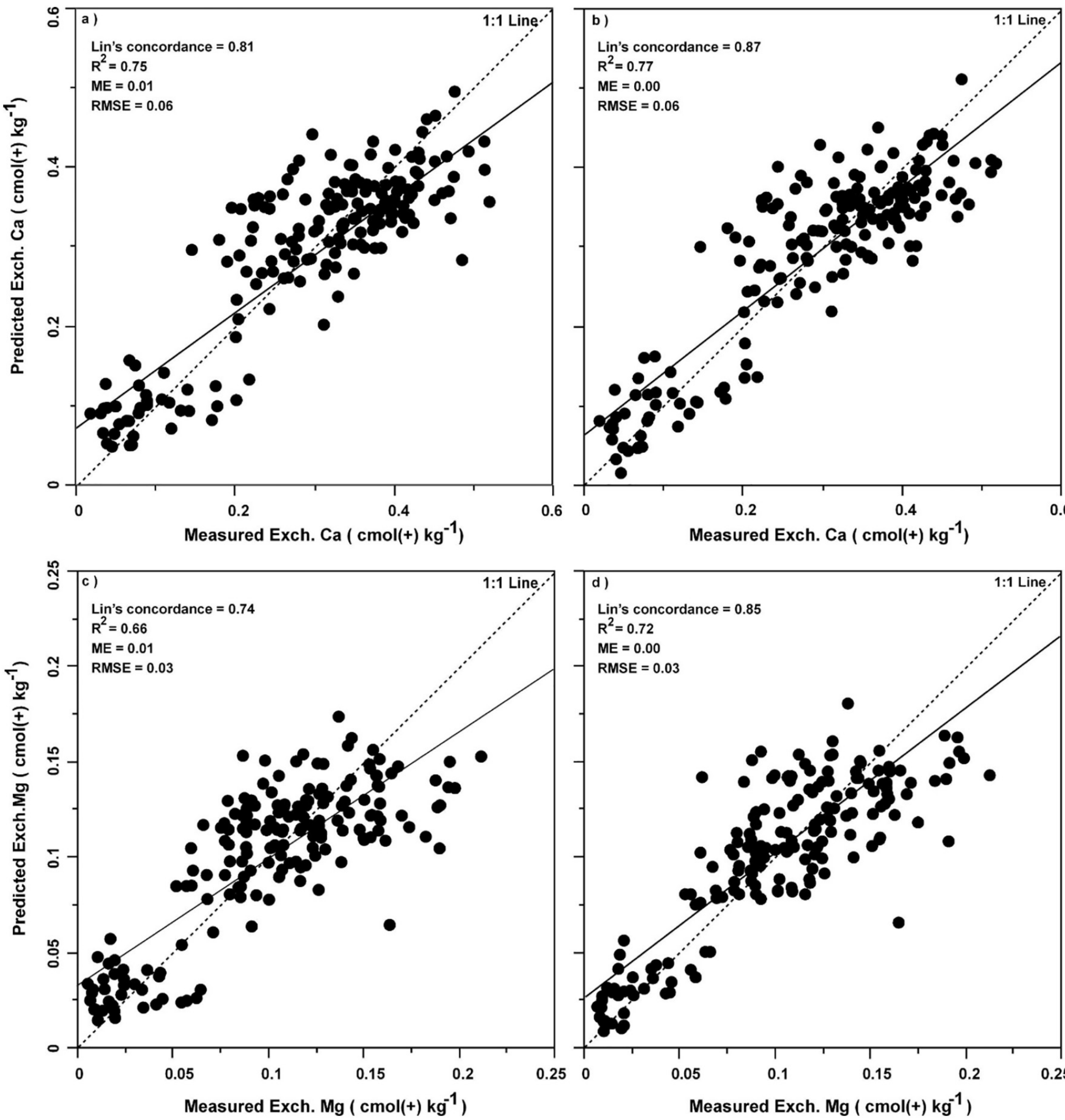

Fig. 6. Plot of measured versus predicted soil exchangeable calcium (Exch. Ca - cmol(+)/kg) using (a) regression kriging (RK) and (b) linear mixed model (LMM) and plot of measured versus predicted soil exchangeable magnesium (Mg - cmol(+)/kg) using (c) regression kriging (RK) and (d) linear mixed model (LMM).

Table 6
Mean squared prediction error (MSPE) of predicted topsoil (0–0.15 m) exchangeable calcium (Exch. Ca - cmol(+)/kg) and magnesium (Exch. Mg - cmol(+)/kg) using regression kriging (RK), linear mixed model (LMM) and Soil Order map and using only the gamma-ray (γ-ray) or apparent electrical conductivity (EC_a) data.

	RK	LMM	Soil order map	γ-ray	EM
Exch. Ca	0.0123	0.0100	0.0171	0.0126	0.0120
Exch. Mg	0.0018	0.0013	0.0024	0.0018	0.0017

the values oscillated between intermediate-small (20–30 mS/m), intermediate (30–40 mS/m) intermediate-large (40–50 mS/m). Fig. 3b shows that the 2mPcon exhibited the same basic pattern while the difference was that the EC_a values were slightly larger by a factor of 2 across the field. The same pattern was evident for the 1mHcon (Fig. 3c) and 2mHcon (Fig. 3d).

We also make note of some anomalous areas where there were bands of smaller EC_a between larger areas of EC_a. This was most evident in the 2mPcon and 1mHcon. These bands were orientated to the northeast and in the most obvious case, coincides with the point of a boundary between two types soil (Chromosols and Vertosols) and approximately in the two-thirds of the way across the field. It was also noteworthy that EC_a increased with the increasing depth of measurement which suggests that the subsoil was more conductive than the topsoil.

3.3. Proximal sensed data selection

To determine which proximal sensed data was useful for RK and LMM approach we conducted a backwards elimination until all predictors had a probability < 0.05. Table 4a shows the summary statistics of selected proximal sensed data and their probability values for predicting Exch. Ca using RK. A total of 4 proximal sensed data, including two γ-ray (U and TC) and two EM (1mPcon and 2mPcon), were selected. Table 4b shows the summary statistics for predicting Exch. Ca using LMM. The optimal proximal data combination includes only one γ-ray (U) and one EM (1mPcon) data. In terms of the EM, the EC_a data

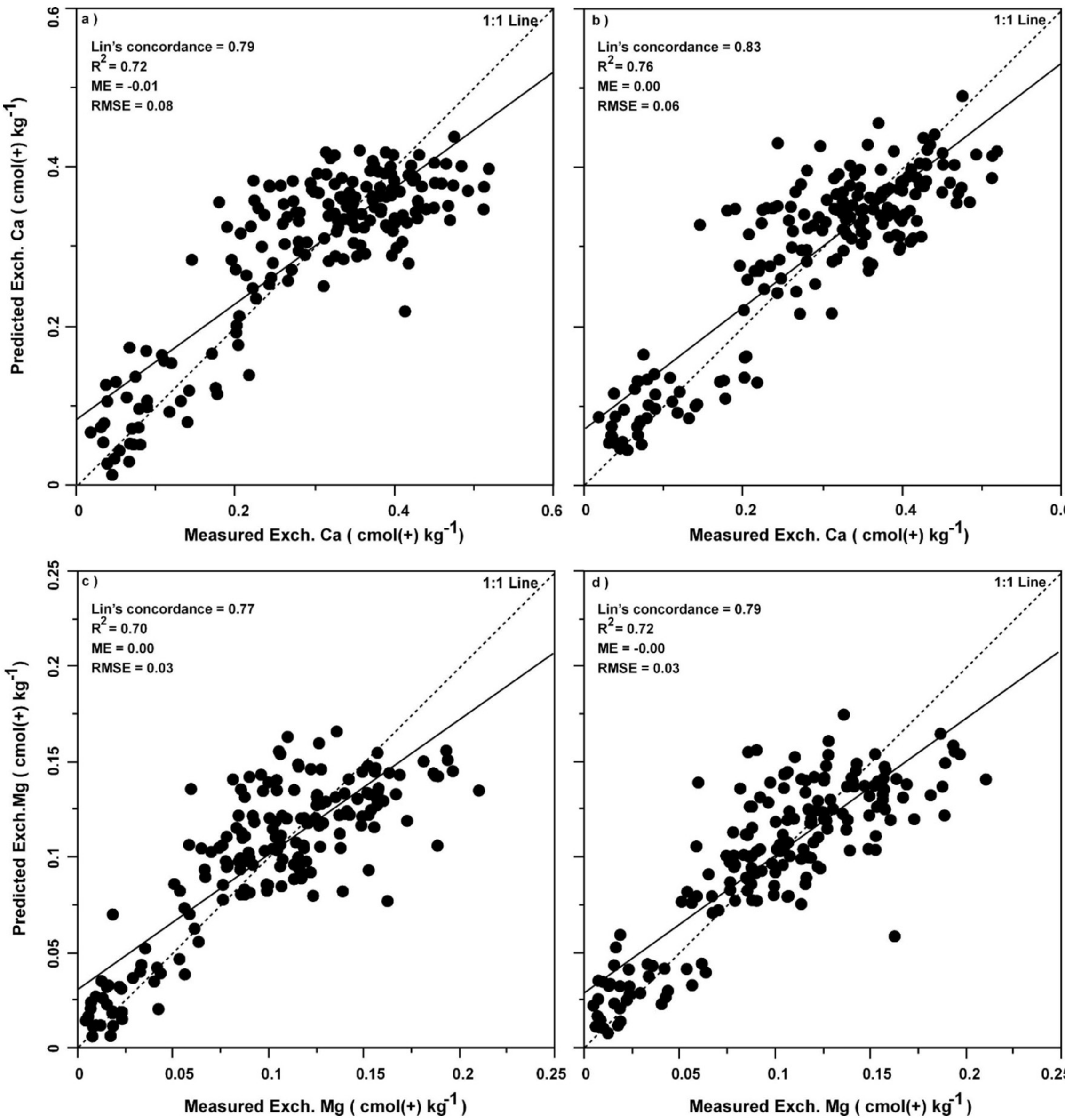

Fig. 7. Plot of measured versus predicted soil exchangeable calcium (Exch. Ca - cmol(+)/kg) by Linear mixed model (LMM) using only proximal sensed (a) gamma-ray (γ-ray) spectrometry and (b) only electrical conductivity (EC_a) data; plot of measured versus predicted soil exchangeable magnesium (Exch. Mg - cmol(+)/kg) by Linear mixed model (LMM) using only proximal sensed (c) gamma-ray (γ-ray) spectrometry and (d) only electrical conductivity (EC_a) data.

selected were the two shallowest measuring arrays.

Table 5a shows the equivalent summary statistics and their probability values for predicting Exch. Mg using RK. Unlike Exch. Ca, the γ-ray signal of TC was not selected, with only U and 1mPcon and 2mPcon necessary. Table 5b shows the summary statistics for predicting Exch. Mg using LMM. As with Exch. Ca only one γ-ray (TC) and one EM (2mPcon) data were required. Interestingly, the former was not selected using the RK approach, and the latter was selected instead of 1mPcon. This is not surprising however given there was a highly significant statistical correlation between Exch. Ca and Mg (Table 2; 0.92) with each other as well as with the all of the proximal sensed data. For example, Exch. Ca was correlated with U (0.49), TC (0.72), 1mPcon (0.85) and 2mPcon (0.83) as shown in Table 2.

3.4. Spatial distribution of predicted Exch. Ca and Mg

Fig. 4a shows predicted topsoil (0–0.15 m) Exch. Ca (cmol(+)/kg) using RK. At the northern end, where the soil was predominantly characterised by topsoil sand or loam textured Chromosols (6Dya), the Exch. Ca was small (< 0.2 cmol(+)/kg). Immediately to the south, where the topsoil texture was sand or loam over sodic clay, or Sodosols (6Dye), the Exch. Ca was intermediate-small (0.2–0.4 cmol(+)/kg). Interspersed among this, however, were contiguous areas of intermediate Exch. Ca (0.4–0.6 cmol(+)/kg). These most likely represent the depressed areas, associated with the Vertosols (2Uge), which were light to light - medium clay and dominates most of the field according to the Soil Order map (Fig. 1b).

Fig. 4c shows the equivalent map of Exch. Ca (cmol(+)/kg) using LMM. The map was similar with that achieved with RK. The implication for nutrient management for Exch. Ca from these maps was clear. Specifically, and according to the Six-Easy-Steps (Table 1), the lime application rate in the northern end of the field should be 3 t/ha given the small (< 0.2 cmol(+)/kg) Exch. Ca. Across the centre and in the south, the lime application rate should be 2.5 t/ha given the Exch. Ca was mostly intermediate-small (0.2–0.4 cmol(+)/kg). However, in a number of isolated and discrete areas, the application should be 2 t/ha given the Exch. Ca was intermediate (0.4–0.6 cmol(+)/kg).

Fig. 5a shows predicted topsoil (0–0.15 m) Exch. Mg (cmol(+)/kg) using RK. Similar patterns of small (< 0.05 cmol(+)/kg), intermediate-small (0.05–0.1 cmol(+)/kg), intermediate (0.1–0.15 cmol(+)/kg) and intermediate-large (0.15–0.2 cmol(+)/kg) were evident. The major difference was the small band of intermediate-small Exch. Mg, between the Chromosols (6Dya) and the Vertosols (2Uge) and demarcated by the Sodosols (6Dye). Another difference was the area delineated as Vertosols was characterised by three classes; including intermediate-small, intermediate and intermediate-large.

Fig. 5c shows the map of predicted topsoil (0–0.15 m) Exch. Mg (cmol(+)/kg) using LMM. The map was similar to the RK map, although it was less affected by short-scale variation. In terms of nutrient management and the application of the Six-Easy-Steps guidelines for Exch. Mg, these maps can be used. According to Table 1, the application rate of magnesium in the northern end, and associated with the Chromosols (6Dya), could be 150 kg/ha given the small Exch. Mg. In the north-east orientated band, associated with the Sodosols (6Dye), the magnesium application rate could be 125 kg/ha given the Exch. Mg was intermediate-small. The magnesium application rate in the various classes identified in the area demarcated as Vertosols (2Uge), should be 125, 100 and 75 kg/ha, depending on intermediate-small, intermediate or intermediate-large Exch. Mg, respectively.

These results and conclusions show how fertilizers can be applied in preference to the ‘one size fits all’ approach. They also potentially show how small variation within established traditional soil maps can be better discerned using a pedometric approach, because the proximal sensed data was able to discern subtle variation within a soil type. Specifically, there were two nutrient management zones discerned for Exch. Ca and three for Exch. Mg. In the case of the former, and considering only the existence of one zone, or soil type (i.e. Vertosols), nutrient management may be inefficient due to under-application or over-application. For example, under-application zones do not reach optimal levels of sugarcane yield whereas over-application areas there will be an increase of costs and high risk of Great Barrier Reef (GBR) lagoon pollution such as runoff with high Exch. Ca or Mg (Haynes et al., 2000).

3.5. Model performance

To better understand these two approaches (i.e. RK and LMM), we also show the maps of the spatial distribution of the RK residuals and LMM errors. Fig. 4b shows the contour plot of the kriged RK residuals on the 5 × 5 m grid. It was apparent, that the residuals were large (> 0.04 cmol(+)/kg) along the western side and mainly within the bounds of the first 6 transects. As we mentioned, in these areas the EC_a data was collected without the use of a stabilising rope to keep the sled carrying the DUALEM-421S instrument positioned directly above the seed bed. As a result, the sled would often derail from the seed bed and slide down into the furrow. The EC_a data was subtly larger therefore and in this part of the field the predicted Exch. Ca was larger. In most other areas, the residual was small (< 0.01 cmol(+)/kg).

Fig. 4d shows the spatial distribution of model errors of LMM for predicting Exch. Ca. The error was large (> 0.08 cmol(+)/kg) in a couple of areas. This was the case along the southern margin, in the area previously delineated by the Sodosols (2Dyb), where intermediate Exch. Ca was predicted. We suggest this error was most likely a function of an edge effect owing to the proximity to the field extent, but also the boundary with a different soil type which was not as well represented compared to a larger one adjacent to it. This was similarly the case in the central parts of the field. Interestingly, boundary effects associated with the band of Sodosols (6Dye) was also evident and between the Chromosols and Vertosols. This was even though there was no specific or obvious change in Exch. Ca between the Sodosol and the Vertosol.

To more directly compare the performance of RK and LMM for Exch. Ca we carried out a leave-one-out cross-validation (Pebesma and Wesseling, 1998). Fig. 6a shows the results for RK, the predictions were shown to be unbiased (ME = 0.01), precise (RMSE = 0.06) and exhibited good concordance (Lin's = 0.81). Fig. 6b showed the results for LMM. The results were equivalent in terms of bias and precision (0.00 and 0.06, respectively), but the concordance was larger (0.87).

These results indicate that the LMM was slightly superior, given also the maximum (0.51 cmol(+)/kg) and minimum (0.02 cmol(+)/kg) predicted Exch. Ca were larger and smaller respectively as compared with RK (0.49 and 0.05 cmol(+)/kg, respectively). The latter is due to the smoothing effect of RK (Hengl et al., 2007). In addition, we calculated the MSPE of both the DSM generated using RK and LMM approaches. In this regard, Table 6 shows the MSPE of LMM DSM (0.01) was smaller than that achieved using RK (0.0123). This also indicates the LMM was more accurate. By way of comparison, the error of the map of Soil Orders was larger (0.0171). These results show that the best map to use to guide nutrient management would therefore be the LMM DSM, followed by the RK map and then the Soil Order map.

Fig. 5b shows the residuals of RK for predicting Exch. Mg. For the most part the residual was small (< 0.01 cmol(+)/kg) across the field. However, along the western side and mainly within the bounds of the first 6 transects shows, the residuals were again large (> 0.04 cmol (+)/kg). We also note that where the Exch. Mg was intermediate-large (0.15–0.2 cmol(+)/kg), the residuals were also intermediate-large or larger (> 0.2 cmol(+)/kg). Fig. 5d shows the spatial distribution of model errors of LMM for predicting Exch. Mg. The pattern was similar pattern with the error for predicting Exch. Ca.

Fig. 6c shows the results of the leave-one-out-cross-validation for RK. The predictions were unbiased (ME = 0.01), precise (0.03) and concordance (Lin's = 0.74). Fig. 6d shows the bias and precision (0.00 and 0.03, respectively) results for LMM. They were equivalent to RK, however the LMM concordance was larger (0.85) and almost as strong as for Exch. Ca. These results indicate clearly that while the RK and LMM approaches were equivalent in terms of bias and precision of prediction, LMM was optimal because of the stronger concordance for both Exch. Ca and Mg.

We again calculated the MSPE of both maps and the Soil Order map. The LMM (MSPE = 0.0013) was smaller than that achieved using RK (0.0018) with the Soil Order map was larger (0.0024). These results again indicate that nutrient management guidelines for Exch. Mg would be the LMM, followed by RK map and then the Soil Order map.

3.6. Proximal sensed data performance

Given the superiority of the LMM approach, we compared which of the proximal sensed data was better at predicting Exch. Ca. Fig. 7a shows the plot of measured versus predicted Exch. Ca using only the γ-ray data. While the predictions were shown to be similarly unbiased (ME = −0.01) and precise (0.08) the concordance was smaller (Lin's = 0.79). Fig. 7b shows the results for the EM data was identical (Fig. 6b) to when both the proximal data were included in the LMM, however the concordance (0.83) was larger than for γ-ray only but smaller than when both sensors were used (0.87).

Fig. 7c shows the plot of measured versus predicted Exch. Mg using only the γ-ray data. Again, the predictions using only γ-ray data were similarly unbiased (0.00) and precise (0.03) compared with using both γ-ray and EC_a data (Fig. 6d), but the concordance was smaller (0.77). Fig. 7d shows the results for the EC_a data was identical to when both the proximal data were included in the LMM (Fig. 6d), however the concordance (0.79) was slightly larger than for γ-ray only but smaller than when both sensors were used.

These results indicate that using the LMM with both proximal sensed data (γ-ray and EM) was optimal with the preference being for the use of EM data over γ-ray data if there was a choice. We also note that the MSPE results conform this given the EM was smaller than for the γ-ray data and as shown in Table 6 for both Exch. Ca and Mg. Interestingly, the MSPE for the EM derived LMM DSM was more accurate than the RK approach and using both proximal sensors. Nevertheless, both sensors either alone or in combination provide DSM where practical soil nutrient guidelines can be applied for lime and magnesium fertiliser requirement across the field and according to the Six-Easy-Steps for Burdekin nutrient management for Exch. Ca and Mg, respectively.

4. Conclusion

We found that proximally sensed γ-ray and EM data, that was collected across an irrigated sugarcane growing field in the Burdekin valley, could be used to establish a relationship with topsoil (0–0.15 m) Exch. Ca and Mg. This was because these cations were correlated with clay and CEC, which were also well correlated with the proximal sensed data. We also showed through a comparison of mathematical modelling approaches, that RK produced predictions of Exch. Ca which were precise (RMSE = 0.06) and unbiased (ME = 0.01) and showed good concordance (Lin's = 0.81). The same was also true for the LMM which was similarly precise and unbiased (0.06 and 0.01, respectively) but was superior given the concordance was larger (0.87). The MSPE of the final LMM DSM (0.01) was also smaller compared to the RK DSM (0.0123). Moreover, both DSM were superior than the traditionally generated map of Soil Orders (0.0171). Equivalent results were the case for Exch. Mg.

In terms of proximal data, the use of U, TC, 1mPcon and 2mPcon were most useful for Exch. Ca with U, 1mPcon and 2mPcon most appropriate for Exch. Mg. We also found that if there was a choice between the two proximal sensed data, the EM data was slightly superior in terms of predicting Exch. Ca than the γ-ray data, however, it would be preferable to use both and in combination. The same results were the case for Exch. Mg. The soil use and management implications of the DSM was also determined, given the fertiliser requirement for Exch. Ca (i.e. lime) and Exch. Mg can be applied in accord with respect to the Six-Easy-Steps for Burdekin nutrient management (Schroeder et al., 2009).

Acknowledgements

The Australian Federal Government's Sugar Research Australia (SRA) is acknowledged for the financial support to conduct the EM and γ-ray surveys, soil sampling, and laboratory analyses. The first author also acknowledges a generous scholarship from SRA. We acknowledge Messer's Sam Lemari, Chris Catchinda, Luke Venables and Andrew Commo who conducted the soil sampling and Michael Sefton and Rod Nielson for technical support. We acknowledge DavCo Farming for providing unrestricted access to the farm and the study field.

References

Bakker, H., 2012. Sugar Cane Cultivation and Management. Springer Science & Business Media.
Beale, S.I., 1999. Enzymes of chlorophyll biosynthesis. Photosynth. Res. 60, 43–73.
Bierwith, P.N., 1996. Gamma - radiometrics, a remote sensing tool for understanding soils. In: Australian Collaborative Land Evaluation Program Newsletter. 5. pp. 12–14.
Bishop, T.F.A., McBratney, A.B., 2001. A comparison of prediction methods for the creation of field - extent soil property maps. Geoderma 103 (1–2), 149–160.
Bristow, K.L., Charlesworth, P.B., McMahon, G.A., Arunakumaren, J., Bajracharya, K., Ham, G., Qureshi, E., 2000. Towards a more integrated approach to water management in the Burdekin Delta irrigation area. In: ANCID Conference, pp. 10–13.
Brus, D., Lark, R.M., 2013. Soil survey. In: El-Shaarawi, A.H. (Ed.), Encyclopaedia of Environmetrics, 2nd edition. John Wiley & Sons.
Christian, C.S., Paterson, S.J., Perry, R.A., Slatyer, R.O., Stewart, G.A., Traves, D.M., 1953. Survey of the Townsville - Bowen Region, North Queensland. pp. 1950.
Donnollan, T.E., McClurg, J.I., Tucker, R.J., 1990. Soils and Land Suitability of Leichhardt Downs Section, Burdekin River Irrigation Area: Detailed Report. Queensland Department of Primary Industries.
Gastal, F., Lemaire, G., 2002. N uptake and distribution in crops: an agronomical and ecophysiological perspective. J. Exp. Bot. 53, 789–799. https://doi.org/10.1093/jexbot/53.370.789.
Grzebisz, W., 2013. Crop response to magnesium fertilization as affected by nitrogen supply. Plant Soil 368 (1–2), 23–39.
Haynes, D., Müller, J., Carter, S., 2000. Pesticide and herbicide residues in sediments and seagrasses from the Great Barrier Reef World Heritage Area and Queensland coast. Mar. Pollut. Bull. 41 (7–12), 279–287.
Hengl, T., Heuvelink, G., Stein, A., 2004. A generic framework for spatial prediction of soil variables based on regression - kriging. Geoderma 122 (1–2), 75–93.
Hengl, T., Heuvelink, G.B., Rossiter, D.G., 2007. About regression - kriging: from equations to case studies. Comput. Geosci. 33 (10), 1301–1315.
Hepler, P.K., 2005. Calcium: a central regulator of plant growth and development. Plant Cell 17, 2142–2155.
Holmgren, G.G., Juve, R.L., Geschwender, R.C., 1977. A mechanically controlled variable rate leaching device 1. Soil Sci. Soc. Am. J. 41 (6), 1207–1208. https://doi.org/10.2136/sssaj1977.03615995004100060041x.
Huang, J., Davies, G.B., Bowd, D., Monteiro Santos, F.A., Triantafilis, J., 2014. Spatial prediction of the exchangeable sodium percentage at multiple depths using electromagnetic inversion modelling. Soil Use Manag. 30 (2), 241–250.
Isbell, R., 2016. The Australian Soil Classification. CSIRO publishing.
Lark, R.M., Cullis, B.R., 2004. Model-based analysis using REML for inference from systematically sampled data on soil. Eur. J. Soil Sci. 55 (4), 799–813. https://doi.org/10.1111/j.1365 - 2389.2004.00637.x.
Lark, R.M., Cullis, B.R., Welham, S.J., 2006. On spatial prediction of soil properties in the presence of a spatial trend: the empirical best linear unbiased predictor (E - BLUP) with REML. Eur. J. Soil Sci. 57, 787–799. https://doi.org/10.1111/j.1365 - 2389.2005.00768.x.
Lawrence, I., Lin, K., 1989. A concordance correlation coefficient to evaluate reproducibility. Biometrics 255–268. https://doi.org/10.2307/2532051.
Li, N., Zare, E., Huang, J., Triantafilis, J., 2018. Mapping soil cation - exchange capacity using Bayesian modeling and proximal sensors at the field scale. Soil Sci. Soc. Am. J. https://doi.org/10.2136/sssaj2017.10.0356.
McBratney, A.B., Santos, M.M., Minasny, B., 2003. On digital soil mapping. Geoderma 117 (1–2), 3–52.
Minasny, B., Hartemink, A.E., 2011. Predicting soil properties in the tropics. Earth Sci. Rev. 106 (1–2), 52–62.
Minasny, B., McBratney, A.B., Whelan, B.M., 2005. VESPER Version 1.62. Australian Centre for Precision Agriculture, McMillan Building A, pp. 5.
Nelson, M.A., Bishop, T.F.A., Triantafilis, J., Odeh, I.O.A., 2011. An error budget for different sources of error in digital soil mapping. Eur. J. Soil Sci. 62 (3), 417–430.
Odeha, I.O.A., McBratney, A.B., Chittleborough, D.J., 1994. Spatial prediction of soil properties from landform attributes derived from a digital elevation model. Geoderma 63 (3–4), 197–214.
Odeha, I.O.A., McBratney, A.B., Chittleborough, D.J., 1995. Further results on prediction of soil properties from terrain attributes: heterotopic cokriging and regression - kriging. Geoderma 67 (3–4), 215–226.
Oliver, M.A., Webster, R., 2014. A tutorial guide to geostatistics: computing and modelling variograms and kriging. Catena 113, 56–69. https://doi.org/10.1016/j.catena.2013.09.006.
Pebesma, E.J., Wesseling, C.G., 1998. Gstat, a program for geostatistical modelling, prediction and simulation. Comput. Geosci. 24 (1), 17–31. https://doi.org/10.1016/S0098 - 3004(97)00082 - 4.
Prosser, I.P., Rustomji, P.K., Priestly, G., Roth, C.H., Post, D., Moran, C.J., Lu, H., 2002. Regional Patterns of Erosion and Sediment Transport in the Burdekin River Catchment. CSIRO Land and Water, Canberra.
Rossel, R.V., Walvoort, D.J.J., McBratney, A.B., Janik, L.J., Skjemstad, J.O., 2006. Visible, near infrared, mid infrared or combined diffuse reflectance spectroscopy for simultaneous assessment of various soil properties. Geoderma 131 (1–2), 59–75.
Schroeder, B., Panitz, J., Wood, A., Kealley, M., 2009. Six-easy-steps nutrient management completed. In: Australian Canegrower, pp. 10–11.
Solymosi, K., Schoefs, B., 2008. Prolamellar body: a unique plastid compartment, which does not only occur in dark-grown leaves. In: Plant Cell Organelles-Selected Topics. Research Signpost, Trivandrum, pp. 151–202.
Stokes, C.J., McAllister, R.R., Ash, A.J., 2006. Fragmentation of Australian rangelands: processes, benefits and risks of changing patterns of land use. Rangel. J. 28 (2), 83–96.
Triantafilis, J., Lesch, S.M., La Lau, K., Buchanan, S.M., 2009. Field level digital soil mapping of cation exchange capacity using electromagnetic induction and a hierarchical spatial regression model. Soil Res. 47 (7), 651–663.
Tucker, B.M., 1974. Laboratory Procedures for Cation Exchange Measurement on Soils, CSIRO Division of Soils Technical Paper No 23.
White, P.J., Broadley, M.R., 2003. Calcium in plants. Ann. Bot. 92 (4), 487–511. https://doi.org/10.1093/aob/mcg164.